JGR Atmospheres

RESEARCH ARTICLE
10.1029/2022JD037824

Key Points:

- Stratospheric extratropical wave forcing is larger in early winter during the easterly quasi-biennial oscillation phase and at solar minimum
- Large wave forcing events in early winter, such as stratospheric warmings, produce a lagged strengthening of the Madden-Julian oscillation (MJO)
- This is therefore a possible mechanism for producing the observed quasi-biennial oscillation and solar modulations of the MJO in winter

Supporting Information:

Supporting Information may be found in the online version of this article.

Correspondence to:

L. L. Hood,
lon@lpl.arizona.edu

Citation:

Hood, L. L., Trencham, N. E., & Galarneau, T. J. Jr. (2023). QBO/solar influences on the tropical Madden-Julian oscillation: A mechanism based on extratropical wave forcing in late fall and early winter. *Journal of Geophysical Research: Atmospheres*, *128*, e2022JD037824. https://doi.org/10.1029/2022JD037824

Received 21 SEP 2022
Accepted 25 FEB 2023

QBO/Solar Influences on the Tropical Madden-Julian Oscillation: A Mechanism Based on Extratropical Wave Forcing in Late Fall and Early Winter

Lon L. Hood[1], Natasha E. Trencham[1], and Thomas J. Galarneau Jr[2]

[1]Lunar and Planetary Laboratory, University of Arizona, Tucson, AZ, USA, [2]NOAA/OAR/National Severe Storms Laboratory, Norman, OK, USA

Abstract Possible sources of the observed modulation of the tropical Madden-Julian oscillation (MJO) by the stratospheric quasi-biennial oscillation (QBO) and the 11-year solar cycle are investigated using 41 years of reanalysis data and archived climate model data. Larger upward fluxes of extratropical planetary-scale waves, leading in some cases to sudden stratospheric warmings (SSWs), are observed in late fall and early winter during the easterly phase of the QBO than during the westerly phase (the "Holton-Tan effect"). A similar but smaller increase occurs, on average, during solar minima relative to solar maxima. In addition to the warming at high latitudes, extratropical wave forcing events produce cooling and reduced static stability in the tropical lower stratosphere. Here, it is found that if SSWs occur in early winter (before ∼mid-January), the reduced static stability produces, on average, a statistically significant, lagged strengthening of the MJO. This therefore represents a possible mechanism for producing, or at least enhancing, the observed QBO and solar modulations of the MJO in boreal winter. An initial analysis of archived climate model data shows that at least one model version with realistic QBO and solar forcing and with $4 \times CO_2$ forcings partly simulates both of these characteristics (QBO/solar modulation of early winter wave forcing and lagged strengthening of the MJO following early winter SSWs). However, the modeled MJO is insufficiently sensitive to QBO-induced static stability reductions, precluding simulation of the QBO-MJO connection.

Plain Language Summary Statistical studies have shown that upper atmospheric conditions significantly modulate the occurrence rate and amplitude of the wintertime Madden-Julian oscillation (MJO), which is a tropical convective disturbance with important consequences for weather events at northern latitudes. Specifically, easterly and westerly winds in the tropical and subtropical stratosphere driven by the quasi-biennial oscillation (QBO) and the 11-year solar cycle influence the amplitude of the MJO in northern winter. Here, it is first found using reanalyzed meteorological data that a statistically significant, lagged strengthening of the MJO is produced, on average, by large-scale waves propagating up from the troposphere in late fall and early winter, leading to a cooling and destabilization of the tropical lowermost stratosphere. Second, more such wave forcing events occur during the easterly phase of the lower stratospheric QBO and at solar minimum. A survey of archived climate model data from a recent model intercomparison project shows that at least one model version with realistic QBO and solar forcing (and high greenhouse gas concentrations) is able to partly simulate both of these characteristics. However, the model fails to simulate the observed stratospheric QBO modulation of the MJO, apparently because the modeled MJO is insufficiently sensitive to stability reductions in the tropical lower stratosphere.

1. Introduction

The tropical Madden-Julian oscillation (MJO) is an eastward propagating, convectively coupled, tropical wave that produces the strongest of the intraseasonal climate oscillations (e.g., Adames & Kim, 2016; Sobel & Maloney, 2012). It generates a Rossby wave train that can be associated with high-impact weather events at northern midlatitudes (e.g., Matthews et al., 2004; Zhang, 2013).

Recent research has found that the stratospheric quasi-biennial oscillation (QBO) (e.g., Baldwin et al., 2001) modulates the occurrence rate and eastward extension of MJO episodes in boreal winter (the "QBO-MJO connection") (e.g., Hood, 2017; Nishimoto & Yoden, 2017; Yoo & Son, 2016; Zhang & Zhang, 2018; see the reviews by Martin, Son, et al., 2021; Haynes et al., 2021). Briefly, the modulation is such that the MJO is stronger for longer time periods, propagates more often across the Maritime Continent into the western Pacific, and is more

predictable when the QBO is in its easterly phase near 50 hPa in the tropical lower stratosphere (QBOE) than when it is in its westerly phase (QBOW). Moreover, several published studies provide evidence for a significant QBO modulation of the strength of the MJO-induced Rossby wave train and associated teleconnection patterns in the extratropics (Hood et al., 2020; Toms et al., 2020). As suggested by Toms et al., the latter modulation may be due in part to a QBO modulation of the tropical MJO itself and in part to the QBO modulation of the extratropical background state that affects the communication of the MJO signal to the extratropics.

As reviewed recently by Haynes et al. (2021; their section 3.1b), Sakaeda et al. (2020) have confirmed that the QBO influence on tropical convection is limited only to the MJO and further demonstrate an increase of MJO high cloud fraction during QBOE, which provides a positive feedback on MJO activity due to cloud-radiative effects on lower stratospheric temperature (see also Giorgetta et al., 1999, for an original model study of cloud-radiative positive feedbacks on QBO-induced convective activity). Abhik and Hendon (2019) suggest that the specific influence of the QBO on the MJO may be due to the higher vertical extent of MJO convection as compared to typical convection combined with unusually cold tropopause temperatures over the Maritime Continent in northern winter.

Evidence that the stratospheric response to 11-year and 27-day solar UV forcing produces a secondary modulation has also been reported (Hoffmann & von Savigny, 2019; Hood, 2017, 2018). The modulation is such that the boreal winter MJO is stronger during solar minima (SMIN) than during solar maxima (SMAX). On the ∼27-day solar rotation time scale, tropical static stabilities are reduced, and strong MJO days are more numerous on average following minima in the solar UV flux. The reverse is found following peaks in the UV flux (see figure 8 of Hood, 2018). The latter effects are mainly limited to strong MJO events (OMI > 2 standard deviations) and are detectable mainly under solar maximum conditions when rotational UV variations are especially large. The solar rotation-induced UV variations occur when active regions are concentrated on one side of the sun; they can be more than half as large as those occurring on the 11-year time scale.

One candidate mechanism for the QBO modulation has been destabilization of the uppermost tropical troposphere and lower stratosphere by the QBO-induced meridional circulation in the tropics and subtropics, which produces relative upwelling and cooling during QBOE, thereby reducing static stability and favoring tropospheric convection. Some idealized model studies and experiments with forecast models have given some support for this mechanism (e.g., Abhik & Hendon, 2019; Martin et al., 2019, 2020).

In boreal winter, another hypothesis involving large-scale stratospheric dynamics for producing the QBO-MJO connection may be considered. It is based on the observed QBO modulation of the occurrence rate of extratropical wave forcing events in early northern winter (e.g., Holton & Tan, 1980, 1982; hereafter referred to as the "Holton-Tan effect" or "H-T"). Previous observational analyses and idealized model experiments have supported both QBO and solar influences on the timing (early winter vs. late winter) of sudden stratospheric warmings (SSWs) via the zonal flow in the equatorial and subtropical stratosphere (e.g., Gray et al., 2004, 2020, 2022). This mechanism would therefore also be potentially applicable to the observed solar modulation of the MJO. Simply stated, extratropical wave forcing events decelerate the polar vortex through a process known as "wave drag", accelerating the effective stratospheric mean meridional circulation. They therefore produce adiabatic descent and higher temperatures in the polar lower stratosphere (e.g., Andrews et al., 1987). At the same time, the tropical upwelling rate is increased and temperatures are decreased in the lower stratosphere, affecting static stabilities and potentially the tropospheric MJO.

Figure 1 shows some evidence that extratropical wave forcing contributes significantly to differences in tropical lower stratospheric temperature (and static stability) between the QBOE and QBOW phases during northern winter when the QBO-MJO connection is mainly observed. Plotted are averages of daily zonal mean temperature anomalies at 70 hPa (deviations from climatology) as a function of latitude for (a) all months of the year; and (b) December through February (DJF). The calculations were done using 40 years of ERA5 reanalysis data (see Section 2 below). The data are separated by QBO phase, where QBOE is defined as periods when the 50 hPa equatorial zonal wind as compiled from radiosonde data at the Free University of Berlin was easterly (u50 < 0) and QBOW as periods when u50 > 0. The 70 hPa level is chosen because the maximum difference between zonal mean equatorial temperature during QBOE and QBOW occurs at this level. It therefore exerts a major QBO influence on static stabilities in the tropical tropopause region. When all months of the year are considered, the tropical equatorial temperature difference is smaller and there is only a very small difference between anomalies at high latitudes. However, when only DJF is considered, the equatorial temperature difference increases substantially and there are corresponding large north polar temperature differences of opposite sign. In both cases, these

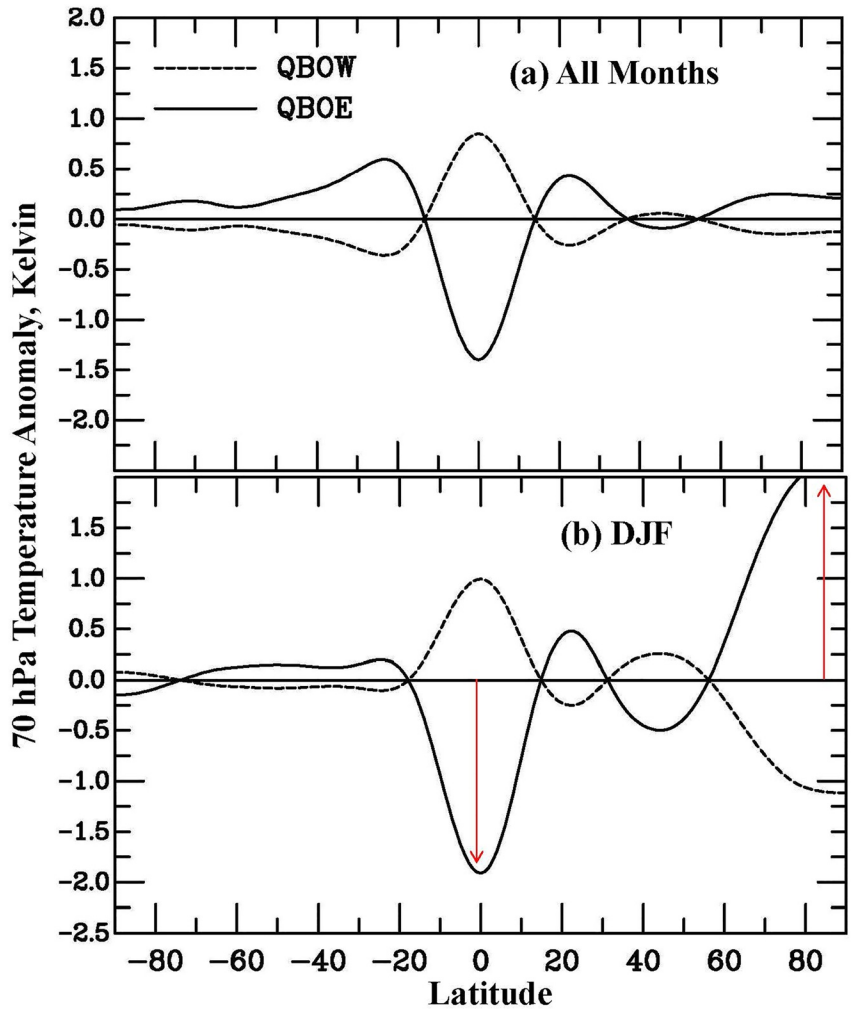

Figure 1. 70 hPa zonal mean temperature anomaly for QBOE years (solid lines) and QBOW years (dashed lines) during (a) all months; and (b) December to February (DJF).

differences are much larger than the two-sigma (~95% confidence) limits (not shown). The opposite-signed anomalies in the tropics and at high northern latitudes are consistent with increased wave drag during QBOE relative to QBOW.

A recent study using an advanced global climate model raises questions about whether any mechanism based on stratospheric dynamics alone could be the source of the QBO-MJO relationship (Martin, Orbe, et al., 2021). The model experiments used "stratospheric nudging," that is, all modeled zonal mean stratospheric zonal and meridional winds were relaxed to reanalysis fields over the 1980 to 2017 period. These experiments therefore should have simulated both the observed QBO-induced meridional circulation at low latitudes and the effect of QBO-induced changes in extratropical wave forcing on the large-scale meridional circulation, tropical upwelling rates, and tropopause static stability during that time period. The model produced a realistic, seasonally averaged, QBO modulation of tropical lower stratospheric temperature (QBOE – QBOW; see their figure 2) but did not simulate a QBO-MJO relationship. Several characteristics of the simulations may have prevented the model from producing a stratospheric effect on the MJO, however. First, as noted by the authors, the modeled MJO was generally weaker and less active around the Maritime Continent as compared to observations. Second, the modeled tropical lower stratospheric temperature in northern winter, which was not nudged to observations, was about 1.9 K too warm at 100 hPa (see their figure 3b and associated discussion).

Another possible criticism of stratospheric dynamics as a source mechanism is that static stabilities are mainly affected by top-down forcing in the 70 to 100 hPa layer, while typical MJO convection does not usually reach

that high. The largest difference in tropical lower stratospheric temperature between QBOE and QBOW occurs at 70 hPa (see, e.g., figure 4b of Kim et al., 2020). In contrast, typical MJO-induced vertical velocity anomalies in northern winter reach the 70 hPa level only over the Maritime Continent region during MJO phases 3–6 (e.g., figure 1 of Hendon & Abhik, 2018, and figure 6 of Martin, Orbe, et al., 2021). However, the latter calculations were done for MJO amplitudes >1 standard deviation, while it is mainly the strongest MJO episodes (amplitudes >2 standard deviations) that are modulated by QBO and solar forcing (see, e.g., figure 6a of Hood, 2018). These episodes may extend to higher altitudes and be more affected by static stability reductions in the lowermost stratosphere.

In this study, we report a more detailed investigation of the hypothesis outlined above that extratropical wave forcing events, including stratospheric warmings, and their timing (early winter vs. late winter) as influenced by QBO and solar forcing, are playing an important role in producing the observed QBO and solar modulations of the MJO. Using 40 years of reanalysis data, we focus especially on the temporal evolution of relevant quantities during the fall and winter seasons as the seasonal minimum in tropical lower stratospheric temperature and static stability is approached. A recent coupled climate model simulation with realistic QBO and solar forcing is then analyzed to evaluate whether it is able to simulate any of the observed effects.

2. Data and Methods

All observational data for atmospheric variables are taken from the ERA5 reanalysis record (Hersbach et al., 2020; see Data Availability Statement). Static stabilities are for the 70 to 100 hPa layer, averaged over near-equatorial latitudes (10°S to 10°N), and are calculated using methods described in Hood (2017). Temperature composites in all figures are done at the 70 hPa level because temperatures at this level exert the main influence on static stabilities in the 70 to 100 hPa portion of the tropical tropopause region. To characterize extratropical wave forcing, zonal mean meridional eddy heat flux ($v'T'$) is calculated at 100 hPa and averaged over northern middle latitudes (45°–75°N). Here, v' is the deviation from the zonal mean of the meridional velocity and T' is the deviation from the zonal mean of the temperature. This quantity is approximately proportional to the vertical component of the planetary-scale wave flux into the stratosphere (e.g., Andrews et al., 1987). "Cumulative" wave forcing in late fall and early winter is calculated as the sum of daily midlatitude-averaged 100 hPa eddy heat fluxes over the October 1 to January 15 period for each year (Table 1, column 8). Cumulative wave forcing in late winter and early spring is calculated as the sum of the same quantity over the January 16 to March 31 period (Table 1, column 9).

To characterize the observed amplitude of the MJO on a given day in the analysis period (1979–2019), we use the outgoing longwave radiation (OLR)-based MJO index (OMI) developed and described in detail by Kiladis et al. (2014). This index requires only satellite OLR data and is provided since 1979 on the online NOAA website, https://psl.noaa.gov/mjo/mjoindex/. OMI amplitudes are normalized such that OMI = 1 represents 1 standard deviation. A listing of the DJF means of OMI for the 40 winters considered here is given in Table 1, column 6.

To select winters that are in the QBOE or QBOW categories, directly measured (radiosonde) equatorial 50 hPa zonal wind monthly means (u50) compiled at the Free University of Berlin are employed (see Data Availability Statement). A plot of the u50 time series for the 1979–2017 period is shown in figure 2 of Hood (2018). To test the sensitivity of the results to the method of assigning a given winter period to the QBOE or QBOW phase, two methods are used.

In Method 1, a "strict" approach was adopted in which only those years when the QBO was in a strongly easterly or westerly state throughout the entire fall-winter period when tropical lower stratospheric temperatures are decreasing to a minimum were accepted. This method also attempts to account for the asymmetry of the wind field (positive winds during QBOW have weaker peak amplitudes than negative winds during QBOE). Specifically, QBOE years are defined as those with monthly mean 50 hPa equatorial zonal winds (u50) during October to January of less than −1 standard deviation (s.d.) and without any monthly value falling below −0.5 s.d. (1 s.d. = 12.8 m/s). Also, to ensure that the QBO phase is continuous throughout the fall, the transition from westerly to easterly is required to occur no later than August of a given year. As shown in Table 1 (column 3), 11 winters qualified as QBOE according to these criteria. For example, the 1994–1995 winter is excluded because u50 increases rapidly in December and January to nearly 0 even though the October–January mean is less than −1 s.d. QBOW years are defined as those with October–January means exceeding 0.6 s.d. but not falling to less than 0.4 s.d. in any of these months. Again, the transition from easterly to westerly must occur no later than

Table 1
QBO/Solar Phases and Related Data of the 40 Winters Considered Here

Winter no.	Winter years	QBO phase Method 1	QBO phase Method 2	Early/Late SSW?	DJF OMI	Solar phase	Heat flux 10/1–1/15	Heat flux 1/16–3/31
1	1979–1980	East	East	Late	0.98	S_{max}	− 139.9	266.9
2	1980–1981	West	West	Late	0.76	S_{max}	− 361.3	223.7
3	1981–1982	–	East	Early	1.52	S_{max}	143.9	− 31.2
4	1982–1983	–	West	–	1.16	S_{max}	− 187.9	169.5
5	1983–1984	–	West	Late	0.68	–	64.7	290.2
6	1984–1985	East	East	Early	2.01	S_{min}	297.2	4.4
7	1985–1986	West	West	–	1.52	S_{min}	97.0	80.3
8	1986–1987	–	West	Late	1.20	S_{min}	11.7	107.0
9	1987–1988	–	West	Early, Late	2.01	–	5.3	57.8
10	1988–1989	West	West	Late	1.39	S_{max}	− 201.0	271.1
11	1989–1990	East	East	–	2.06	S_{max}	− 70.8	− 290.7
12	1990–1991	West	West	–	0.95	S_{max}	− 75.1	199.9
13	1991–1992	–	East	–	1.59	S_{max}	236.4	149.8
14	1992–1993	–	West	–	1.77	–	− 111.1	50.0
15	1993–1994	West	West	–	1.10	–	264.8	− 181.2
16	1994–1995	–	East	–	1.60	S_{min}	− 106.5	− 56.0
17	1995–1996	West	West	–	1.13	S_{min}	− 192.4	153.0
18	1996–1997	East	East	–	2.05	S_{min}	147.0	− 506.4
19	1997–1998	West	West	–	0.90	–	230.9	18.1
20	1998–1999	East	East	Early, Late	1.24	–	99.5	68.4
21	1999–2000	West	West	Late	0.71	S_{max}	− 177.0	− 37.5
22	2000–2001	–	West	Late	1.61	S_{max}	68.3	69.4
23	2001–2002	East	East	Early, Late	1.66	S_{max}	242.9	− 251.0
24	2002–2003	–	West	Late	1.60	–	170.7	3.5
25	2003–2004	East	East	Early	1.98	–	358.4	− 233.0
26	2004–2005	–	West	–	1.00	–	− 113.2	315.1
27	2005–2006	East	East	Late	1.41	S_{min}	190.5	− 109.7
28	2006–2007	West	West	Late	1.37	S_{min}	− 53.1	104.7
29	2007–2008	East	East	Late	2.32	S_{min}	34.0	57.1
30	2008–2009	West	West	Late	1.01	S_{min}	− 6.7	154.0
31	2009–2010	West	West	Late	1.38	S_{min}	121.1	304.6
32	2010–2011	–	West	–	0.69	–	3.8	− 312.7
33	2011–2012	–	West	–	1.44	–	76.4	15.8
34	2012–2013	East	East	Early	1.50	–	249.2	− 379.9
35	2013–2014	West	West	–	0.98	S_{max}	− 68.9	121.9
36	2014–2015	–	East	–	1.20	–	153.4	− 243.7
37	2015–2016	–	West	–	1.76	–	− 268.3	416.7
38	2016–2017	–	West	–	1.02	S_{min}	86.6	− 26.7
39	2017–2018	–	West	Late	1.68	S_{min}	− 41.2	180.5
40	2018–2019	East	East	Early	1.89	S_{min}	447.5	− 81.4

August. The 12 qualifying QBOW winters are also identified in Table 1, column 3. According to this method, 17 of 40 winters did not qualify as either QBOE or QBOW.

In Method 2, a "relaxed" approach is used in which any winter (December–February or "DJF") season with a mean value of u50 that is greater than zero is assigned as QBOW while a winter with mean u50 less than 0 is assigned as QBOE. As shown in Table 1, column 4, 15 winters qualified as QBOE and 25 winters qualified as QBOW according to these criteria.

To select winters that are in the SMIN or SMAX categories, we use the observed (i.e., unadjusted for varying sun-Earth distance) solar radio flux at 10.7 cm wavelength (F10.7). This emission originates in the vicinity of sunspots and is an objective ground-based proxy for solar ultraviolet emissions at wavelengths that are important for ozone production and radiative heating in the tropical upper stratosphere. A daily and monthly record of F10.7 beginning in 2004 was obtained from the solar radio monitoring program at Dominion Radio Astrophysical Observatory in Penticton, British Columbia, a program operated by the National Research Council of Canada (https://spaceweather.gc.ca/forecast-prevision/solar-solaire/solarflux/sx-5-en.php). We use this proxy record instead of direct measurements and models of solar ultraviolet emissions because of its objectivity and length (1947–present), which allows application to both the observational time period (1979–2019) and the MRI model simulation period (1961–2000). It correlates closely with the solar UV flux at wavelengths near 200 nm (e.g., figure S5 of Hood, 2016). F10.7 is given in solar flux units (1 flux unit = 10^{-22} W m^{-2} Hz^{-1}). SMIN winters are defined here as those with F10.7 < 85 flux units, while SMAX winters are defined as those with F10.7 > 150 flux units. As listed in Table 1 for the 1979–2019 period, 14 winters qualified as SMIN and 12 winters qualified as SMAX. Fourteen winters did not qualify as either SMIN or SMAX.

A compositing method is used to investigate whether the temporal evolution of a given quantity (e.g., MJO amplitude) in a given atmospheric state (e.g., QBOE) differs significantly from that in an alternate state (e.g., QBOW). To evaluate this, 95% confidence limits of the daily means must first be calculated. If the corresponding daily mean of the alternate atmospheric state falls outside of these limits, then the means are considered to be significantly different from one another on that day (see, e.g., Figure 2). Because the number of available years for compositing in the 41-year record is small (typically <30 in a given atmospheric state), confidence intervals are calculated using a method designed for small sample sizes (LaMorte, 2021). Specifically, if $\overline{x}$ is the mean value on a given day, the 95% confidence interval is defined as $\overline{x} \pm t\,(\sigma/\sqrt{n})$, where σ is the standard deviation and n is the number of samples. t is a value calculated from a t-distribution, which is similar to the standard normal distribution but adjusted to account for smaller sample sizes. The calculated t value depends on the degrees of freedom, defined as $n - 1$, and is tabulated in the above reference.

As noted above, the OLR MJO Index (OMI) is a measure of the MJO's activity level on a given day (Kiladis et al., 2014). In order to calculate daily OMI amplitudes from a given set of climate model data, we use a Python package produced by Hoffmann et al. (2021) and available from http://dx.doi.org/10.5281/zenodo.3613752. The initial inputs to the calculation are daily outgoing long-wavelength radiation (OLR) values between 20°S and 20°N. These values are first filtered to accept only eastward propagation at periods between 30 and 96 days. Then, using many years of data (e.g., 40), the two leading-order empirical orthogonal functions (EOFs) are calculated for each day of the calendar year. Finally, the 20–96 days filtered OLR values are projected onto the daily EOFs. The resulting principal component (PC) pairs are given the labels OMI_1 and OMI_2 and the total OMI amplitude is calculated as $OMI = [OMI_1^2 + OMI_2^2]^{1/2}$. When calculating OMI amplitudes from climate model data, one could in principle use either EOFs derived from the climate model data or the observed EOFs (basically the same as those computed by Kiladis et al., 2014). The former approach could lead to problems if the model-derived EOFs change significantly during a long simulation. Therefore, in our work, we have projected the model bandpass-filtered data onto the observed OMI EOFs.

Finally, as listed in Table 2, the central dates of SSWs occurring during the study period (1979–2019) are selected based on compilations given by Charlton and Polvani (2007), Butler et al. (2017), and Karpechko (2018) with the addition of two more recent sudden warmings occurring in 2018 and 2019 (Rao et al., 2019, and references therein). Twenty-six sudden warmings occurred during the considered 40 winters although many other minor warmings could also have been identified.

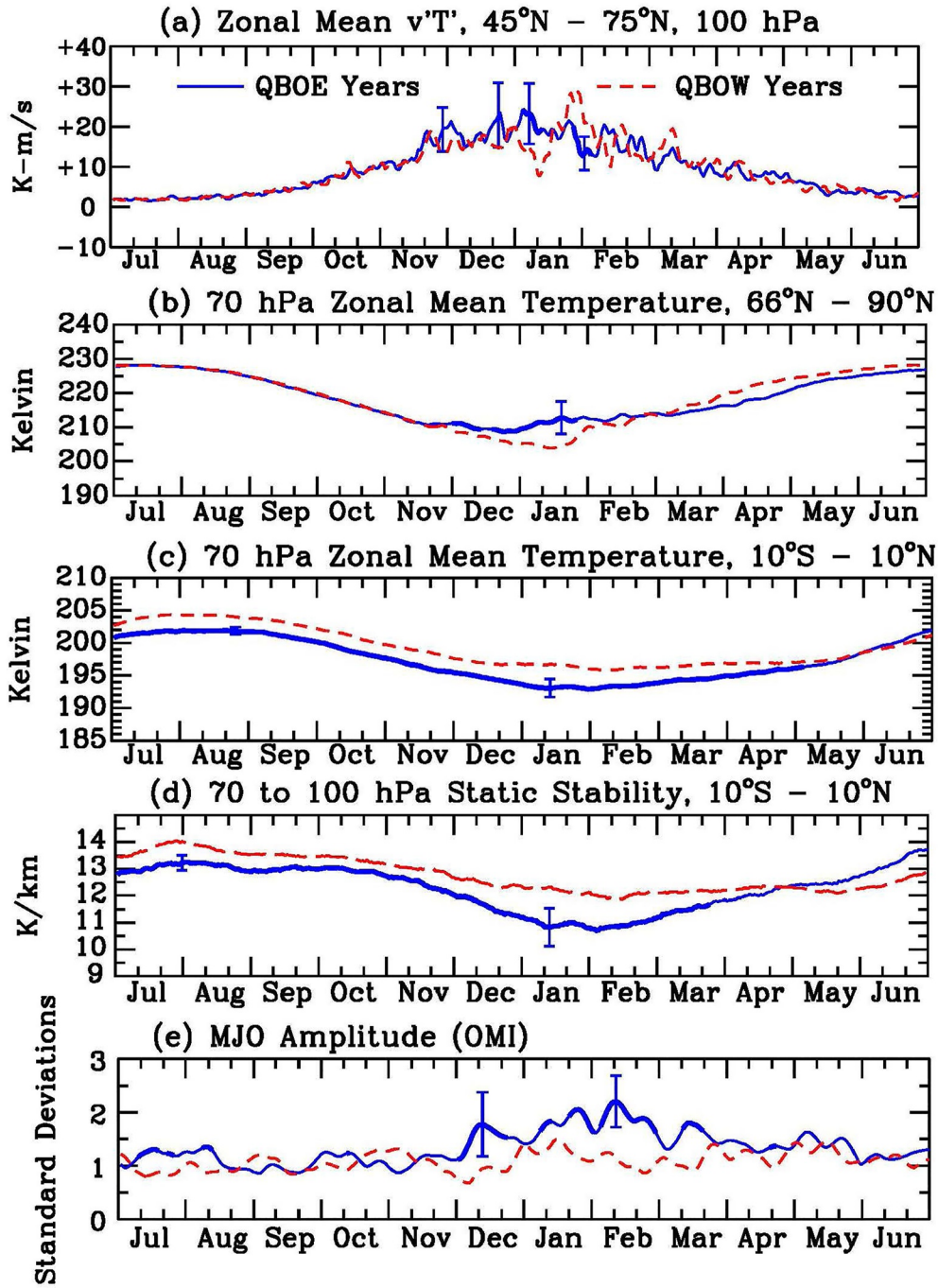

Figure 2. The blue solid lines are daily composites of the indicated quantities during 11 QBOE years selected according to the strict Method 1 (Table 1). The red dashed lines are similar daily composites but for 12 QBOW years selected according to the same method. Heavy lines indicate significance according to criteria given in Section 2. Representative error bars are shown.

3. Increased Early Winter Wave Forcing and MJO Amplitudes in QBOE and SMIN

The absorption and dissipation of extratropical Rossby and gravity waves originating in the troposphere, acting to decelerate the stratospheric zonal flow during northern winter, is referred to here as extratropical wave forcing (e.g., Holton et al., 1995). The resulting drag of these westward propagating waves on the zonal flow produces via the Coriolis torque an acceleration of the mean meridional residual circulation in the stratosphere (the Brewer-Dobson circulation). The most extreme examples of extratropical wave forcing events are SSWs, which produce both

Table 2
Recognized Sudden Stratospheric Warmings During 1979–2019

SSW no.	Central date	Early/Late winter	QBO phase Method 1	QBO phase Method 2	Solar phase
1	February 22, 1979	Late	West	West	–
2	February 29, 1980	Late	East	East	Max
3	March 4, 1981	Late	West	West	Max
4	December 4, 1981	Early	–	East	Max
5	February 24, 1984	Late	–	West	–
6	January 1, 1985	Early	East	East	Min
7	January 23, 1987	Late	–	West	Min
8	December 7, 1987	Early	–	West	–
9	March 14, 1988	Late	–	West	–
10	February 21, 1989	Late	West	West	Max
11	December 15, 1998	Early	East	East	–
12	February 26, 1999	Late	East	East	–
13	March 20, 2000	Late	West	West	Max
14	February 11, 2001	Late	–	West	Max
15	December 30, 2001	Early	East	East	Max
16	February 17, 2002	Late	East	East	Max
17	January 18, 2003	Late	–	West	–
18	January 5, 2004	Early	East	East	–
19	January 21, 2006	Late	East	East	Min
20	February 24, 2007	Late	West	West	Min
21	February 22, 2008	Late	East	East	Min
22	January 24, 2009	Late	West	West	Min
23	February 9, 2010	Late	West	West	Min
24	January 7, 2013	Early	East	East	–
25	February 12, 2018	Late	–	West	Min
26	January 2, 2019	Early	East	East	Min

strong warming at polar latitudes (e.g., Charlton & Polvani, 2007) and pronounced cooling in the tropical lower stratosphere (e.g., Chandra, 1986; Fritz & Soules, 1970; Hood & Soukharev, 2003; Randel, 1993; Randel et al., 2002; Yoshida & Yamazaki, 2011). Planetary-scale waves are strongest in the Northern Hemisphere and are able to propagate into the stratosphere mainly during the boreal winter season, when stratospheric winds are westerly in an acceptable range (Charney & Drazin, 1961). This, combined with a relatively long (~100 days) radiative timescale, produces in the tropical lower stratosphere a large annual temperature cycle with a seasonal minimum in temperature in boreal winter (e.g., Randel et al., 2002).

As mentioned in the Introduction, it has been known since the work of Holton and Tan (1980, 1982) that lower stratospheric planetary-scale waves in the extratropics have higher amplitudes in early northern winter during the easterly phase of the QBO than in the westerly phase (the "Holton-Tan effect"). The explanation suggested by them involved a northward shift of the zero wind line and therefore of the effective waveguide for extratropical planetary-scale waves. This would concentrate wave activity in the northern polar region (Figure S1a in Supporting Information S1), thereby weakening the vortex and strengthening the residual meridional circulation. There has been some support for this mechanism but much debate and the exact origin of the Holton-Tan effect continues to be the subject of ongoing research (Elsbury et al., 2021; Lu et al., 2020; Rao et al., 2020; Silverman et al., 2021; Watson & Gray, 2014; White et al., 2016). It has further been recognized since the work of Labitzke (1982, 1987) and Labitzke and van Loon (1988) that major SSWs do not usually occur in early winter under SMAX conditions, but tend to be delayed until late winter, implying a secondary solar influence on the strength of extratropical wave forcing. A possible mechanism for the suppression of early winter SSWs at SMAX is increased UV heating of the tropical upper stratosphere near winter solstice, leading to a strengthening of the stratopause westerly jet (Kodera & Kuroda, 2002; see their figure 15). If so, then increased wave forcing and SSWs in early winter during QBOE and SMIN would lead to relative tropical upwelling, potentially contributing to wintertime lower stratospheric static stability reductions and tropospheric MJO amplitude increases (Figures S1a and S1b in Supporting Information S1).

Figure 2 shows the results of composite analyses conducted to investigate the mean annual temporal evolution during the two phases of the QBO of: (a) the upward flux of planetary-scale waves into the high-latitude stratosphere as measured by meridional eddy heat flux at 100 hPa; 70 hPa temperatures averaged over (b) polar latitudes and (c) near-equatorial latitudes; (d) static stability in the 70 to 100 hPa layer averaged over near-equatorial latitudes; and (e) MJO amplitude. See Section 2 for data sources. As shown in the top panel of the figure, wave forcing tends to be larger during QBOE (blue lines) than during QBOW (red dashed lines) in several periods before mid-January, but becomes significantly less after this time (see Lu et al., 2020, for detailed investigation of the "sign-reversal" of the Holton-Tan effect in midwinter). As shown in panel (b), 70 hPa zonal mean temperature at high latitudes is larger during QBOE than during QBOW for most of December, January, and February (DJF). As shown in panels (c) and (d), equatorial 70 hPa temperatures and 70 to 100 hPa static stabilities are lower during QBOE than during QBOW throughout the late summer and fall seasons, but are especially low during DJF. Finally, as shown in panel (e), MJO amplitudes are significantly larger during QBOE than during QBOW during DJF. Results using the relaxed Method 2 of QBO phase selection (Figure S2 in Supporting Information S1) are qualitatively consistent with those of Figure 2.

The continuously lower 70 hPa tropical temperatures and static stabilities during QBOE in the July to November period in Figures 2c and 2d are partly attributable to increased upwelling associated with the QBO-induced meridional circulation, which operates more or less independently of season. However, September to Novem-

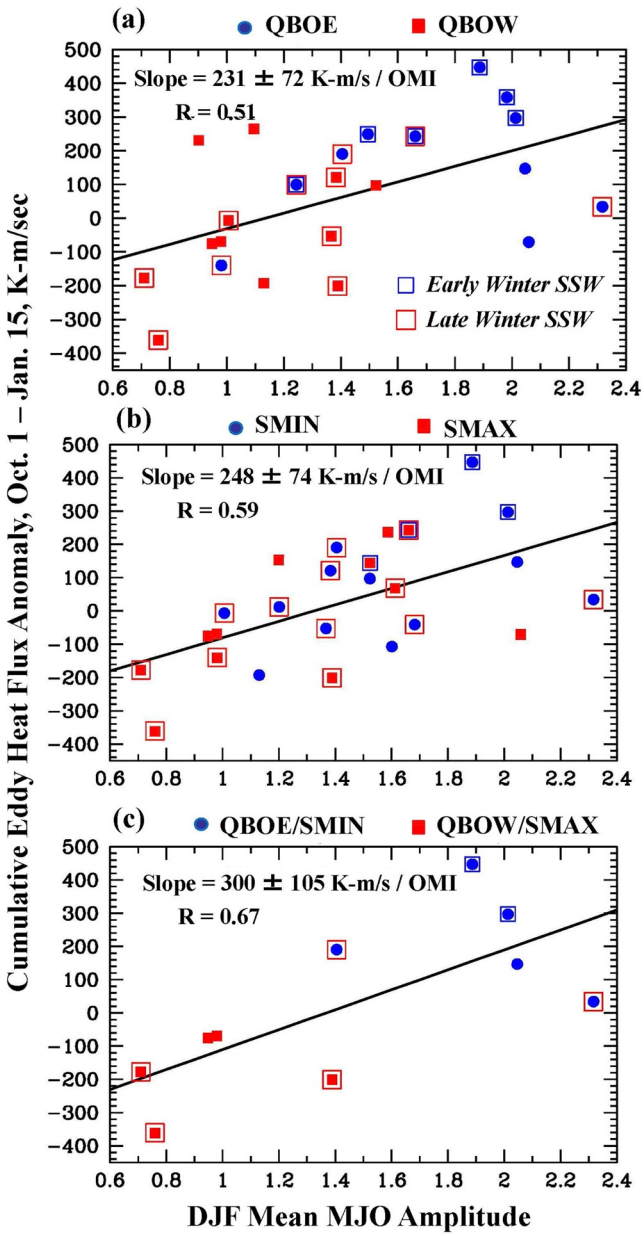

Figure 3. A measure of extratropical wave forcing in late fall and early winter (see the text) is plotted versus December to February (DJF) mean OMI Madden-Julian oscillation (MJO) amplitude for (a) QBOE and QBOW winters (Method 1); (b) SMIN and SMAX winters; and (c) combined QBOE/SMIN and QBOW/SMAX winters.

ber is also the time when the Southern Hemisphere undergoes extratropical wave forcing and exhibits significantly larger wave amplitudes in QBOE than in QBOW (Holton & Tan, 1980). So, some combination of these factors may be responsible for the lower static stabilities in QBOE before December. Southern Hemisphere wave forcing in November may even contribute to the tropical temperature decrease in DJF shown in Figure 2c (see, e.g., Fueglistaler et al., 2014). Future work should therefore probably calculate the sum of Southern and Northern Hemispheric wave fluxes rather than Northern Hemispheric fluxes only, as is done in Figure 2a. However, the increased high-latitude QBOE 70 hPa temperatures during DJF in Figure 2b, and the especially low QBOE 70 hPa tropical temperatures and static stabilities during that season seen in Figures 2c and 2d, strongly suggest that increased Northern Hemispheric wave forcing events in late November, December, and early January are mainly responsible for the 70 hPa temperature decrease in DJF, acting to further destabilize the tropical lowermost stratosphere.

To investigate this possibility further, Figure 3a plots the cumulative anomalous wave forcing in late fall and early winter against the mean DJF MJO amplitude for the QBOE and QBOW years selected according to the strict Method 1 (an alternate analysis using Method 2 is shown in Figure S3 in Supporting Information S1). As explained in Section 2, the early winter anomalous wave forcing is estimated by summing over the October 1 to January 15 period for each year the daily meridional eddy heat flux anomalies (i.e., deviations from the climatological mean), averaged over latitudes from 45°N to 75°N. A positive correlation and a positive slope are obtained. One standard deviation error estimates for the regression slopes are given in the figure. All slopes are positive at the two standard deviation levels (~95% confidence). Alternatively, if cumulative anomalous wave forcing in late winter (summed over the January 16 to March 31 period) is plotted against mean DJF MJO amplitude for the same years, a negative correlation and a negative slope are obtained (Figure S4 in Supporting Information S1). This reflects the tendency seen in Figure 2a for anomalously large wave forcing in early winter to be compensated by anomalously weak wave forcing in late winter, and vice versa (see Lu et al., 2020, for further discussion).

Figure 4 is a composite analysis as in Figure 2, but comparing composites for SMIN and SMAX years (column 7 of Table 1). Although not as clear as for the QBO composites in Figure 2, a tendency for wave forcing during SMIN years to be stronger in early winter (before the end of January) than in late winter can be seen in Figure 4a. Static stabilities are somewhat lower in midwinter during SMIN (Figure 4d) and MJO amplitudes are somewhat larger in several midwinter periods during SMIN than during SMAX (Figure 4e).

Figure 3b is as in Figure 3a but for years selected as SMIN and SMAX. A positive correlation and a positive slope are again obtained. Figure 3c is as in Figures 3a and 3b but for years selected using Method 1 as both QBOE and SMIN or QBOW and SMAX (Table 1). Although only 5 years in each category are available, a somewhat higher correlation is obtained. As shown in Figure S5 in Supporting Information S1, markedly larger composited differences are also obtained, although in the case of MJO amplitude (Figure S5e in Supporting Information S1), these are only significant in some time periods due to the wider confidence intervals.

Blue (red) square outlines are added in Figure 3 to years when an early (late) winter SSW occurred (defined as occurring prior to or after 15 January, respectively). A listing of all SSWs during the study period was given in Table 2 of Section 2. As shown in column 5 of Table 1, 6 of the 12 Method 1 QBOW years had late winter warmings while none had early winter warmings. Four of the 11 Method 1 QBOE years had early winter SSWs,

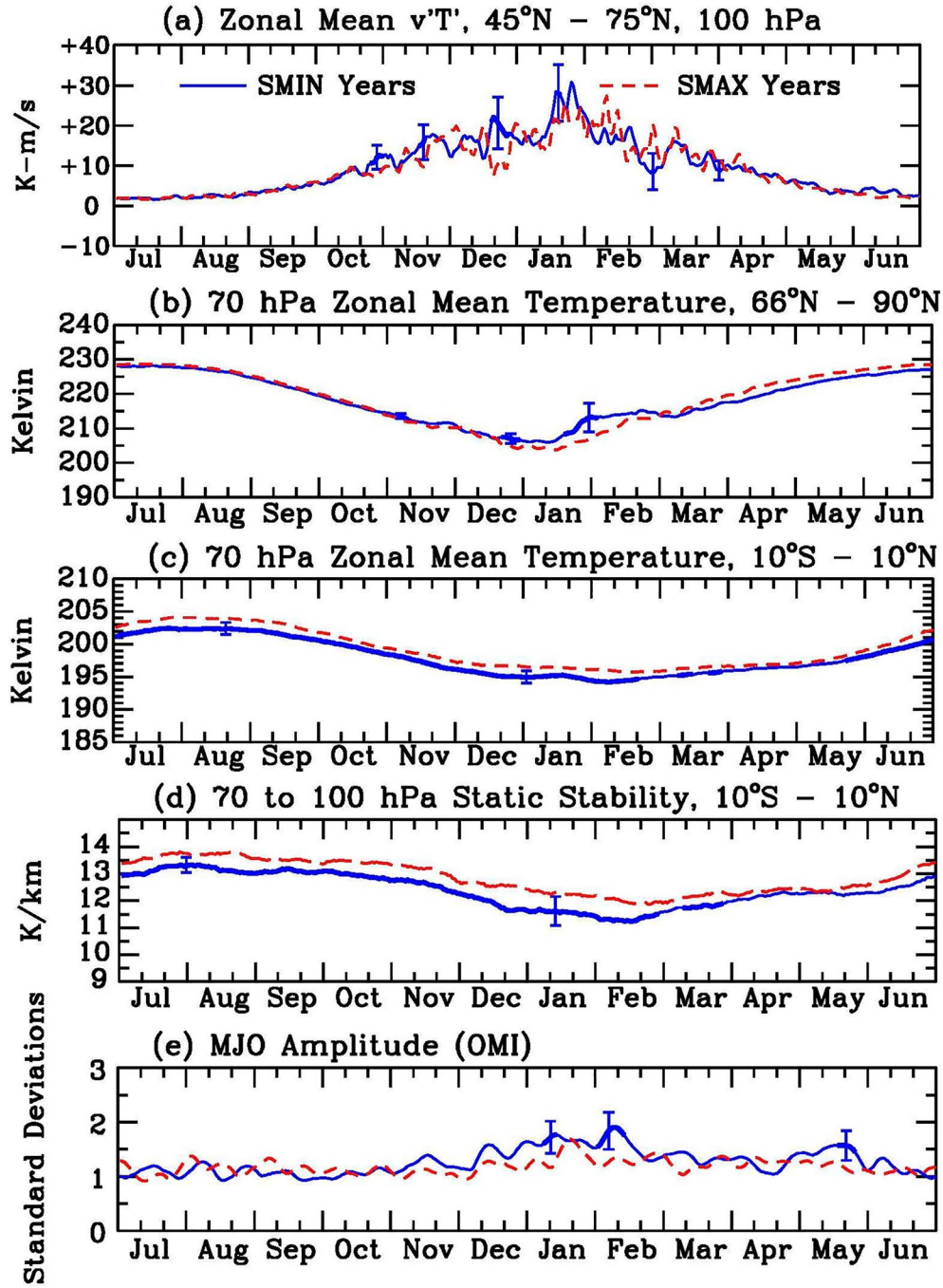

Figure 4. As in Figure 2 but comparing composites for 14 SMIN years versus 12 SMAX years as listed in Table 1.

2 had both early and late winter SSWs, and 3 had late winter SSWs. Therefore, if only the Method 1 QBO years are considered, early winter SSWs only occurred during QBOE while late winter SSWs occurred mainly during QBOW.

Figure 5 presents further evidence from the ERA5 data set that early winter wave forcing is influenced by both the QBO (Holton-Tan) and the 11-year solar cycle. It plots the cumulative anomalous wave forcing in early winter against (a) the DJF mean equatorial 50 hPa zonal wind, u50, and (b) the DJF mean solar radio flux at 10.7 cm (F10.7; see Section 2). Those winters qualifying as QBOE and QBOW according to Method 1 and as SMIN and

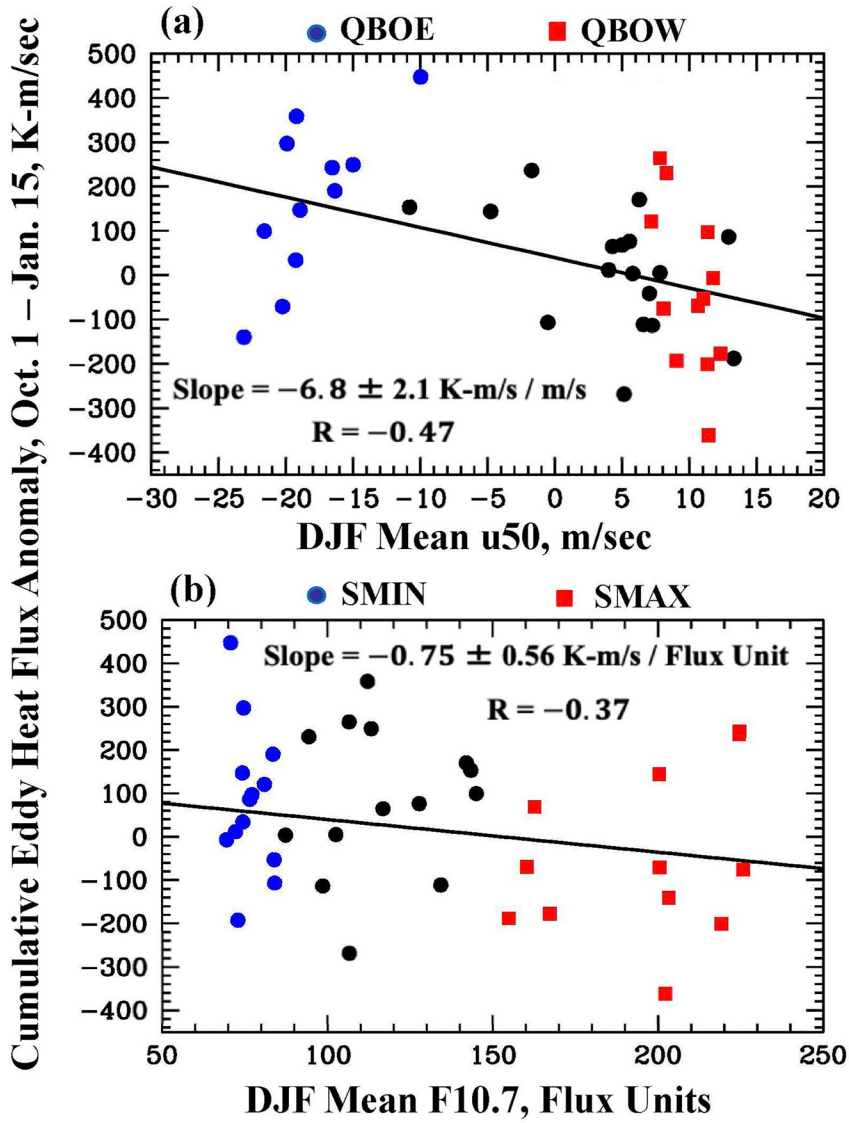

Figure 5. Evidence for quasi-biennial oscillation (QBO) and solar influences on extratropical wave forcing in early winter. The early winter anomalous wave forcing (Section 2) is plotted against (a) December to February (DJF) mean u50 and (b) DJF mean F10.7.

SMAX are highlighted. Only those winters are considered in the regression and cross-correlation results shown in the figure. Significant trends toward reduced wave forcing with increasing u50 and F10.7 are obtained.

4. Is There a Response of the MJO to SSWs in Early Winter?

Although a correlation between early winter extratropical wave forcing and DJF MJO amplitude was shown in Figure 3a, it could be argued that the correlation is only a result of those two processes being separately influenced by the QBO. To investigate further whether extratropical wave forcing can be a cause of the increased MJO amplitudes in QBOE, individual case studies are needed. Since SSWs are the strongest and most well-defined individual wave forcing events, and since early winter SSWs are found only during QBOE when Method 1 is used, we evaluate here the static stability and MJO response to SSWs in early winter.

The blue lines in Figure 6 show the results of composite analyses similar to those of Figure 2 but for days before and after the central dates of all SSWs that occurred on or before January 15 in the 1979–2019 period (eight SSWs; Table 2). The early winter SSW daily composites are compared to daily annual composites for 18 years

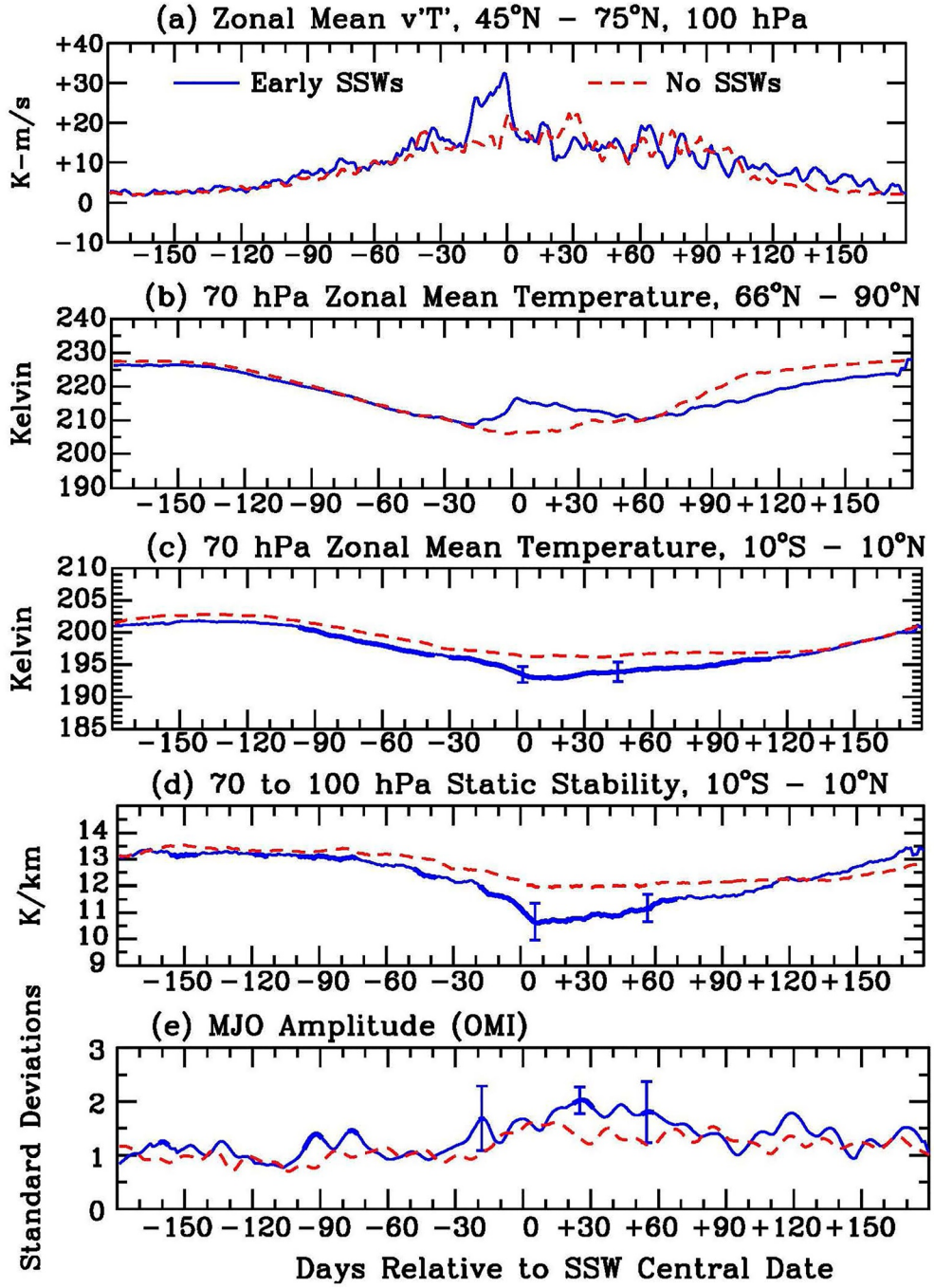

Figure 6. As in Figure 2 but the blue solid lines are daily composites of the indicated quantities relative to the central dates of eight sudden stratospheric warmings (SSWs) occurring in early winter (by January 15, Table 2). The red dashed lines are daily composites of the same quantities relative to January 1 (the assumed "central date") of 18 years with no SSWs (see the text).

with no SSWs (red dashed lines). We used January 1 as an arbitrary "central date" for years with no SSWs. Repetitions of the analysis using the average central dates of the early winter SSWs as the effective central date for years with no SSWs produce a negligible change in the results.

As shown in Figure 6a, the mean peak wave forcing occurs at or just before the central dates of the early winter SSW group. As shown in the (b) and (c) parts, the early winter group produces an immediate warming at higher latitudes and a smaller cooling at equatorial latitudes. As shown in part (d), there is a corresponding sharp

reduction in static stability immediately following the central date of the early group. Finally, part (e) shows that there is a statistically significant difference in MJO amplitudes peaking about 25 days (on average) after the central date for the early winter SSW group that does not occur in years with no SSWs. As also seen in part (e), several other short periods of apparent significance occur at random times during the composite. This is to be expected because significant results can be obtained 5% of the time at random locations during a composite by chance alone. The main evidence in Figure 6 for a real lagged response of the MJO to SSWs is the occurrence of a prolonged period of higher MJO amplitude, part of which is formally significant, following the SSW central date that does not occur in years with no SSWs. These results are not very sensitive to the exact choice of January 15 as the midwinter dividing date. For example, choosing January 21 instead yields two additional SSWs, but the composited results change only slightly.

We note that a previous study by Kodera (2006) also found evidence for anomalous convective activity in the tropical troposphere following major and minor stratospheric warmings in 1979–2001, that is, enhanced convection south of the equator and suppressed convection north of the equator. However, his study did not separate the warmings into early and late winter groups and did not investigate effects on the MJO.

Figures S6–S13 in Supporting Information S1 plot the annual time series for each of the 8 years with early winter SSWs. Considerable interannual variability is evident but, in most cases, an increase in MJO amplitude occurs following the SSW. Repetitions of the analysis, in which the early winter SSW composites are compared to composites of 15 years with SSWs only in late winter, yield larger differences in MJO amplitude after the central dates (Figure S14 in Supporting Information S1). In contrast, repetitions in which all 26 SSWs are considered, regardless of their timing in a given winter, yield no statistically significant lagged difference in MJO amplitude (Figure S15 in Supporting Information S1). It is noteworthy that a statistically significant composited increase in MJO amplitude is obtained in the latter case at several times prior to the SSW central date, including at about − 30 days (Figure S15e in Supporting Information S1). This may be consistent with previous findings that a strong MJO event can sometimes be a precursor to a boreal winter SSW through its effect on tropospheric planetary-scale waves (Garfinkel et al., 2012, 2014; Wang & Tziperman, 2018).

5. Initial Model Comparisons

A recent assessment by Kim et al. (2020) of the representation of the QBO-MJO connection in models participating in the Coupled Model Intercomparison Project 6 (CMIP6) (Eyring et al., 2016) has found that none of them simulates a statistically significant difference in MJO activity between QBOE and QBOW during DJF (see also Lee & Klingaman, 2018; Martin, Son, et al., 2021). As concluded by the authors, this may be due to a lack of complete realism of many of the model QBOs, that is, a weaker amplitude of the QBO than observed, especially between 100 and 50 hPa. It should be emphasized that a successful simulation of the connection also depends on the realism of the MJO in the model, which can be sensitive to the details of the convective parameterization (e.g., Chen et al., 2021). Two of the models considered by Kim et al. (E3SM-1-0 and MRI-ESM2.0) did simulate a realistic QBO temperature difference at 70 hPa in the equatorial lowermost stratosphere, which should have helped to destabilize tropical convection, but still did not produce a significant effect on the MJO in DJF. Here, we examine in more detail archived CMIP6 simulations using one of these models (MRI-ESM2.0; Yukimoto et al., 2019), which is available with daily output at the required vertical resolution. In addition to the simulation using historical forcings, we also consider a $4 \times CO_2$ simulation, which results in increased radiative cooling and reduced climatological static stabilities in the tropical lower stratosphere. A more detailed examination of CMIP6 model simulations will be given in a future publication.

Table S1 in Supporting Information S1 lists the QBO phases of 39 model winters during the first ensemble member of the historical simulation, determined according to Methods 1 and 2, while Table S2 in Supporting Information S1 lists the central dates of SSWs that occurred during the same model winters using the selection criteria of Charlton and Polvani (2007). Tables S3 and S4 in Supporting Information S1 list the same information for 40 winters of the first ensemble member of the $4 \times CO_2$ simulation.

Fewer early winter warmings (5 over a 40-year period) occurred in the historical MRI model simulation than occurred in the ERA5 record (8 over a 41-year period). Nevertheless, a composite analysis (analogous to that done for Figure 6) was done comparing the 5 years with early winter SSWs versus the 17 years with no SSWs. Results are shown in Figure S16 in Supporting Information S1. The (a) and (b) parts agree qualitatively with the corresponding ERA5 results of Figure 6. There is also a statistically significant reduction of 70 hPa temperature

to a minimum of ~197K following the central date as shown in part (c), somewhat weaker than is obtained in Figure 6c (minimum ~194K). A statistically significant static stability reduction also occurs following the central date as seen in Figure S16d in Supporting Information S1. However, the static stability remains rather high (~12.4K/km) compared to what is obtained from the observed early winter warmings in Figure 6d (~10.9K/km). No significant model MJO response following the early winter MRI SSWs listed in Table S4 in Supporting Information S1 is obtained (Figure S16e in Supporting Information S1).

We have therefore conducted a similar composite analysis for the $4 \times CO_2$ simulation, which has lower climatological static stabilities, owing to CO_2 cooling. We first considered only the 40 model winters listed in Tables S3 and S4 in Supporting Information S1. However, only five early winter SSWs again occurred versus 21 years with no SSWs. As shown in Figure S17 in Supporting Information S1, a mean increase in MJO amplitude is obtained near and following the time of the early winter SSW central date. However, the most significant response occurred just before the central date and there is a concern that five early winter SSWs may not be a sufficiently large sample. Therefore, the analysis was expanded to consider three full ensemble members, each covering 151 years from 1850 to 2000. These three members are designated as r1, r4, and r7 in the CMIP6 archive. A statistically significant strengthening of the modeled MJO following the SSW central date is obtained in two of the three members. In the case of the first ensemble member, designated r1, 24 early winter SSWs occurred versus 70 years with no SSWs. Composited results are shown in Figure 7, yielding a significant strengthening of the MJO 10–15 days after the central date. A similar strengthening at a lag of about 15 days is also obtained when analyzing the third (r7) ensemble member (Figure S18 in Supporting Information S1). Overall, the lagged MJO strengthening following early winter SSWs in the MRI model, while statistically more robust, appears to be somewhat weaker and occurs at a shorter time lag than that obtained from the (admittedly small) sample of eight observed SSWs in the previous section.

To investigate the dependence of the modeled MJO strengthening on the depth of the static stability reduction following an SSW, all three ensemble members were considered together (450 model winters), yielding a total of 72 early winter SSWs. The 72 SSWs were then divided into two groups, one that produced relatively large static stability reductions and one that produced relatively weak reductions. Specifically, static stabilities during the 10 days following the central dates were compared to those during a reference period from 15 to 6 days before the central dates. Differences between the two time periods defined the depth of the static stability reduction. SSWs that produced relatively large static stability reductions (more than -0.7K/km) were composited separately from those that produced relatively weak (less than -0.7K/km) reductions. As shown in the (a) and (b) parts of Figure 8, the large reduction composite yielded a pronounced strengthening of the MJO peaking about 12 days after the central date. In contrast, as shown in the (c) and (d) parts, the weak reduction composite yielded no statistically significant increase in MJO amplitude following the central date. This indicates that the lagged strengthening of the MJO in the MRI model following early winter SSWs occurs primarily when the SSW produces a relatively large tropical static stability reduction.

Finally, it is of interest to investigate whether the archived MRI model data show any evidence for a QBO modulation of the MJO. Figure S19 in Supporting Information S1 shows a composite analysis of the 9 Method 1 QBOE model years of the historical MRI simulation versus the 19 Method 1 QBOW model years, done in the same way as for Figure 2. As shown in part (a), wave forcing in early winter is larger on average for the QBOE years. As shown in column 5 of Table S3 in Supporting Information S1, 11 of the 19 QBOW years had late winter SSWs, while none had early winter SSWs. So, there is some agreement of this MRI model simulation with the observed Holton-Tan relationship. Further evidence that this is the case is shown in Figure S20a in Supporting Information S1, which plots modeled anomalous early winter wave forcing against DJF mean u50. As shown in Figure S20b in Supporting Information S1, which plots modeled anomalous early winter wave forcing against DJF mean F10.7, the MRI model simulation also simulates a solar influence on early winter wave forcing (compare with Figure 5b). Nevertheless, as shown in the remainder of Figure S19 in Supporting Information S1, there is a much less pronounced decrease in tropical lower stratospheric temperature and static stability during QBOE than is found in observations, and no detectable increase of MJO amplitude in winter or spring during QBOE relative to QBOW (Figure S19e in Supporting Information S1).

Considering the three full ensemble members of the MRI $4 \times CO_2$ simulation, no convincing evidence of a QBO modulation of the modeled MJO is again obtained. Figure S21 in Supporting Information S1 shows a composite analysis of 34 Method 1 QBOE winters versus 26 Method 1 QBOW winters from the r1 ensemble member. Of the 34 QBOE winters, 5 had early winter SSWs and 11 had late winter SSWs. Of the 26 QBOW winters, one had an early winter SSW while 13 had late winter SSWs. This is consistent with a partial H-T

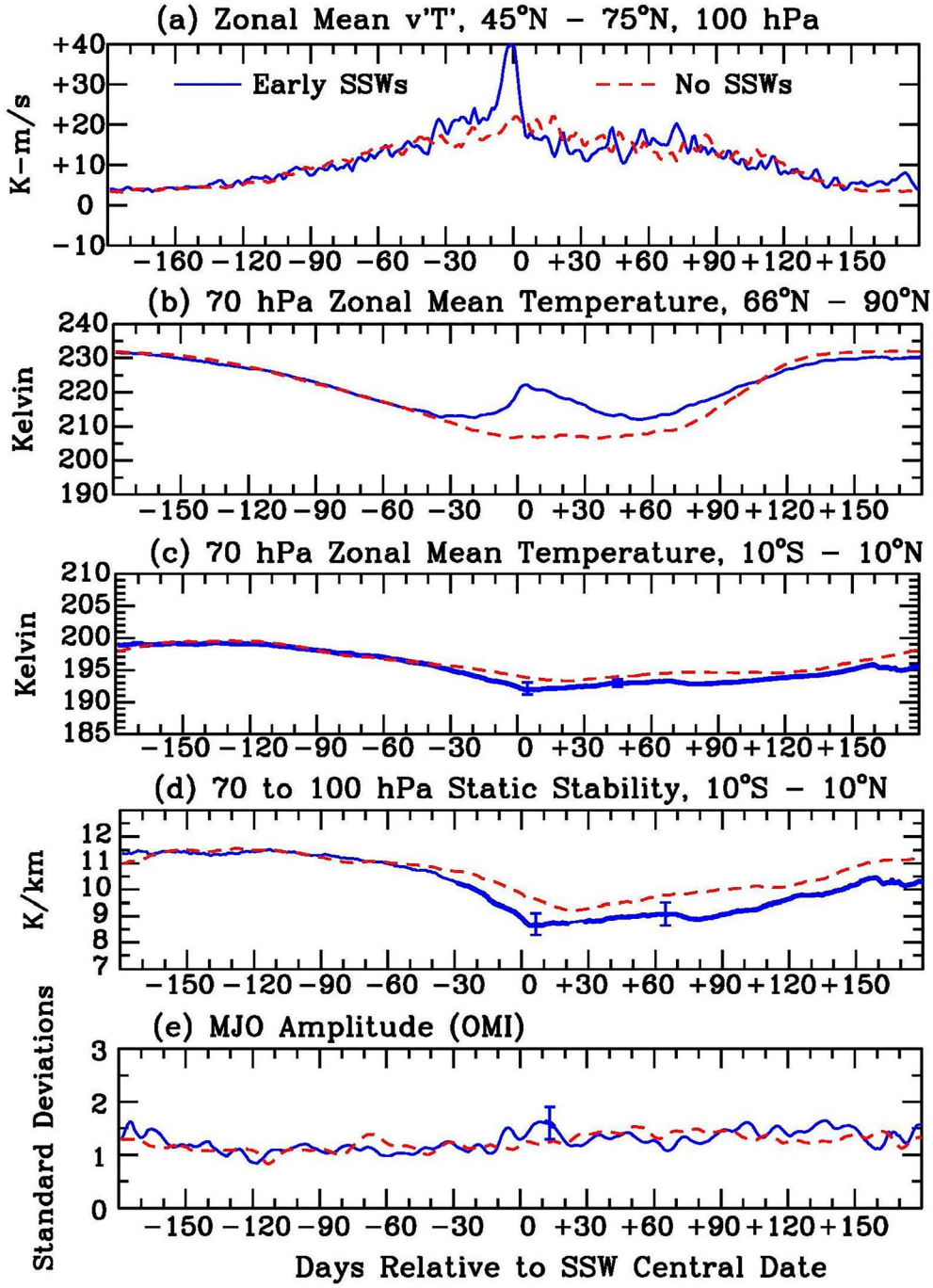

Figure 7. As in Figure 6 but comparing a composite of 24 early winter sudden stratospheric warmings (SSWs) occurring in the r1 ensemble member of the MRI 4 × CO_2 model simulation (blue lines) versus a composite of 70 model winters with no SSWs (red dashed lines).

effect in the model, as already indicated in Figure S20 in Supporting Information S1. As shown in Figure S21d in Supporting Information S1, this model version produces a larger static stability reduction in midwinter than does the historical forcings version (compared with Figure S19d in Supporting Information S1). As shown in Figure S21e in Supporting Information S1, while there is some evidence for an increase in MJO amplitude during QBOE relative to QBOW at limited times in boreal winter and spring, there is no persistent increase in boreal winter as found in observations. As shown in Figures S22 and S23 in Supporting Information S1, similar results are obtained when analyzing the other two ensemble members (r4 and r7), neither of which yield

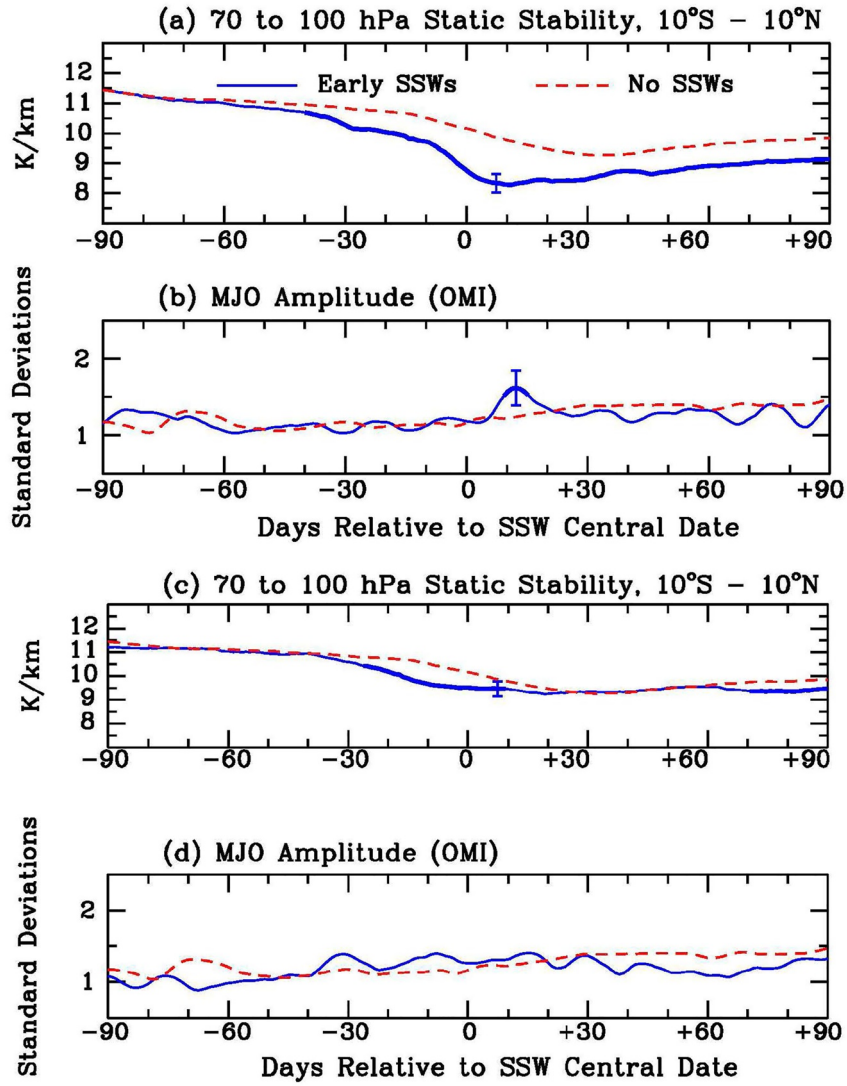

Figure 8. Comparison of effects on Madden-Julian oscillation (MJO) amplitude of sudden stratospheric warmings (SSWs) in the MRI model that produce strong and weak reductions of tropical lower stratospheric static stability. The (a) and (b) parts are for the strong reduction case, while the (c) and (d) parts are for the weak reduction case (see the text for details).

a significant QBO modulation of the MJO that persists for more than a short time period. Therefore, for both the historical simulation and the $4 \times CO_2$ simulation, no positive evidence is obtained in agreement with the conclusions of Kim et al. (2020).

To investigate possible reasons why the hypothesized mechanism is unable to simulate a QBO-MJO connection in the MRI model, it is useful to consider separately the individual components of the mechanism. This is done for the r1 ensemble member of the $4 \times CO_2$ model version in Figure 9. Figure 9a plots the cumulative October 1 to January 15 extratropical meridional eddy heat flux anomalies versus DJF mean tropical 70 to 100 hPa static stability for those model years that qualified as Method 1 QBOE (blue filled circles) or Method 1 QBOW (red filled squares). As was done for the observational results in Figure 3, winters with an early winter SSW are enclosed in a blue box, while those with late winter SSWs are enclosed in a red box. It is evident from the figure that QBOE winters tend to lie more toward the upper left of the diagram (higher early winter wave fluxes and lower tropical static stability), while QBOW winters are more often found in the lower right part of the diagram. Five of the QBOE winters have early winter SSWs, while only one of the QBOW winters had an early winter SSW. Late winter SSWs occur more often during QBOW. This is again consistent with the existence of a partial Holton-Tan effect in the model and also indicates that static stabilities tend to be reduced in QBOE years relative to QBOW years.

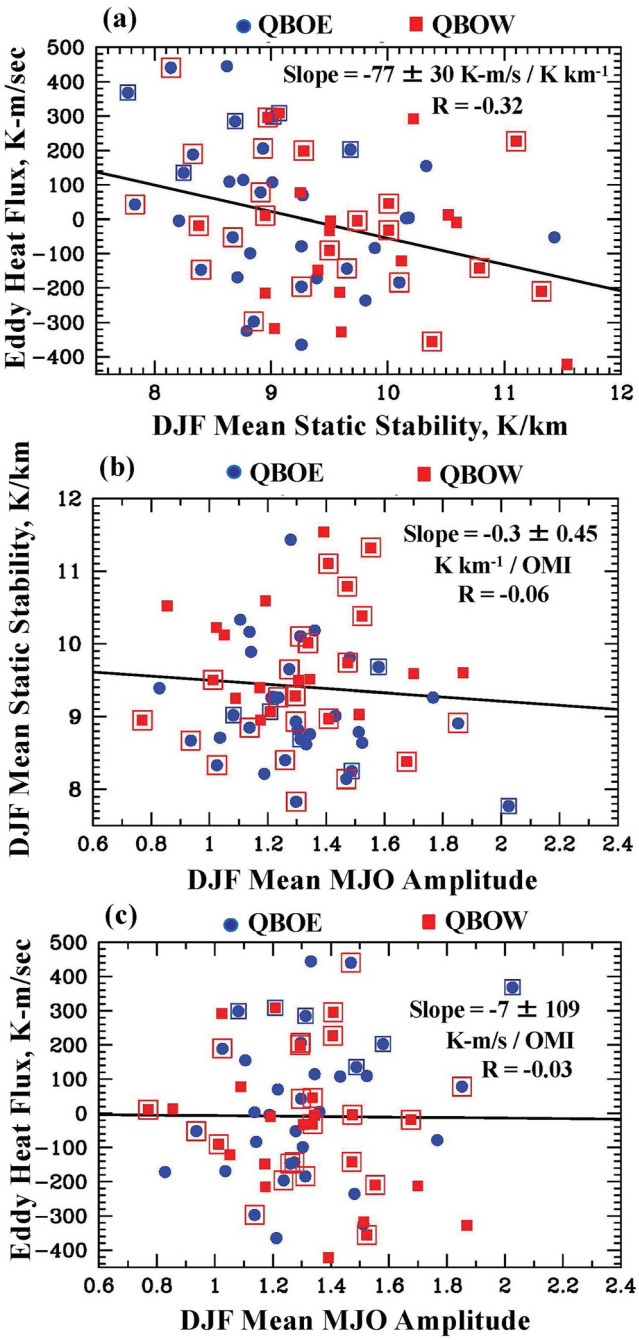

Figure 9. Cumulative October 1 to January 15 eddy heat flux anomalies are plotted against December to February (DJF) mean 70 to 100 hPa 10°S to 10°N static stabilities for all winters in the MRI 4 × CO_2 r1 ensemble member that qualified as Method 1 QBOE or QBOW; (b) as in (a) but plotting DJF mean static stabilities against DJF mean Madden-Julian oscillation (MJO) OMI amplitude; (c) as in (a) but plotting the heat flux anomalies against DJF mean MJO amplitude. Regression line slopes, one sigma errors, and correlation coefficients (R) are given.

However, as shown in Figure 9b, the static stability reductions in QBOE do not produce significantly higher DJF mean MJO amplitudes. There is no overall correlation between DJF mean 70 to 100 hPa static stability and MJO amplitude, unlike what is seen in the available observational record (e.g., Yoo & Son, 2016, their figure 4b). Consequently, Figure 9c shows no correlation between the cumulative early winter eddy heat flux and DJF mean MJO amplitude, unlike what was obtained observationally in Figure 3a.

6. Summary and Conclusions

While the observational sample size for this study (40 winters) is limited, several conclusions based on the available data may be stated. The composite analyses of Section 3 (Figures 2 and 3) show that negative cumulative late fall/early winter eddy heat flux anomalies more often than not portend a less-than-average MJO amplitude winter, while positive anomalies portend a greater-than-average MJO amplitude winter. A major SSW occurring in early winter (before ~January 15) is typically associated with a strong MJO winter. Positive early winter meridional eddy heat flux anomalies tend to be associated with QBOE and SMIN years, while negative anomalies are more often associated with QBOW and SMAX years (Figures 3–5). These stratospheric influences are superposed on a myriad of influences originating in the troposphere-ocean system. It is therefore not surprising that some years do not fit well into this simplified picture.

The evidence from Figure 6 and Figure S14 in Supporting Information S1 (Section 4) is that early winter SSWs produce, on average, a lagged amplification of MJO activity through their effect on tropical lower stratospheric static stability, while late winter SSWs produce no detectable amplification. The estimated lag time based on 8–10 events in the study period is about 25 days after the SSW central date. If this is verified with future data, a causal relationship is implied between an extratropical wave forcing event (here an SSW) in late fall/early winter, a subsequent reduction in tropical lower stratospheric static stability, and a lagged increase in MJO amplitude following the wave forcing event. Six of the eight early winter SSWs analyzed here occurred when the QBO was in a strictly easterly phase (Method 1). So, it is possible that the occurrence of the SSW during a strictly QBOE early winter is a factor in producing a stronger lagged MJO response. It is possible that the timing of the event in early winter, when 70 hPa temperatures are already decreasing toward a minimum, produces lower static stabilities than can occur following a late winter SSW, when 70 hPa temperatures and static stabilities are already higher and rising. Positive feedbacks from MJO convection-induced temperature anomalies (Hendon & Abhik, 2018), cloud-radiative effects (e.g., Giorgetta et al., 1999; Sakaeda et al., 2020), and increased tropospheric Rossby wave amplitudes acting to further accelerate the Brewer-Dobson circulation and tropical upwelling rates, may further enhance MJO amplitudes.

As discussed in Section 5, an initial analysis of model simulations from the CMIP6 archive for a model (MRI-ESM2.0) with realistic QBO and solar forcing yields some positive results. An analysis of 40 years of the model simulation with historical forcings shows that it partly simulates the observed (Holton-Tan) increased early winter wave forcing during QBOE (Figure S20a in Supporting Information S1), the lack of early winter SSWs during QBOW (Table S1 in Supporting Information S1), the observed increased early winter wave forcing during SMIN (Figure S20b in Supporting Information S1), and the reduction of tropical lower stratospheric temperature and static stability following early winter SSWs (Figure S16c and S16d in Supporting Information S1). However, it does not simulate the observed depth of the seasonal climatological minimum in

tropical static stability, produces no lagged MJO response to early winter SSWs (Figure S16e in Supporting Information S1), and produces no QBO modulation of the MJO (Figure S19 in Supporting Information S1).

A more detailed analysis was therefore conducted of three full ensemble members (453 model years) of the MRI simulation with 4 × CO_2 forcings. This model version has lower climatological tropical static stabilities and is able to simulate a significant lagged strengthening of the modeled MJO following the central dates of relatively strong early winter SSWs. This was found to be true in composite analyses of two of the three analyzed ensemble members (Figure 7 and Figure S18 in Supporting Information S1). However, the modeled MJO strengthening appears to be somewhat weaker and the estimated lag time (12–15 days) is shorter than that estimated from the (admittedly limited) sample of 8–10 SSWs in the available record. This difference in time lag could reflect a real delay in the observed MJO response, due to positive feedbacks mentioned above that may not be accounted for fully in the model. Or it could simply be an inaccurate measure of the true time lag due to the limited available sample of early winter SSWs.

As shown in Figure 8, only those SSWs that produced relatively strong tropical static stability reductions were able to produce a significant lagged MJO strengthening. In our view, this supports the static stability mechanism for producing a top-down influence on the MJO in the model.

None of the three analyzed ensemble members of the 4 × CO_2 MRI model simulations shows a significant increased MJO amplitude during QBOE relative to QBOW except for short time periods at random times, which could occur by chance alone (Figures S21, S22, and S23 in Supporting Information S1).

Possible reasons for the lack of a QBO-MJO connection via the hypothesized mechanism considered here in the MRI model were therefore investigated. As shown in Figure 9a, the modeled partial Holton-Tan effect produces, on average, larger early winter extratropical wave fluxes in QBOE relative to QBOW. These larger fluxes produce tropical upwelling rate changes which, combined with those resulting from the QBO-induced meridional circulation, lead to reduced tropical lower stratospheric static stabilities in QBOE than in QBOW. However, as shown in Figure 9b, the static stability reductions in QBOE produce a negligible increase in the modeled MJO amplitude. This lack of sensitivity of the modeled MJO to tropical static stability reductions precludes any overall effect of the QBO on MJO amplitude, as shown in Figure 9c. It also likely weakens the lagged strengthening of the modeled MJO following early winter SSWS such that only events producing relatively large static stability reductions are able to produce a significant strengthening (Figure 8). More detailed analyses of the MRI model data are needed to determine the exact reasons for this lack of sensitivity. It is possible, for example, that the modeled MJO is insufficiently strong or has too few strong episodes (OMI > 2) to be affected by lower stratospheric static stability reductions.

Data Availability Statement

ERA5 reanalysis data were downloaded from https://doi.org/10.24381/cds.bd0915c6. The OLR-based MJO index (OMI) data were obtained from www.esrl.noaa.gov/psd/mjo/mjoindex. The directly measured u50 QBO wind field data are available for download from www.geo.fu-berlin.de/en/met/ag/strat/produkte/qbo/index.html. The 10.7 cm solar radio flux ground-based proxy for solar UV variability is available from https://spaceweather.gc.ca/forecast-prevision/solar-solaire/solarflux/sx-5-en.php. MRI-ESM2.0 model data are available from the U.S. Dept of Energy CMIP6 archive site (https://esgf-node.llnl.gov/search/cmip6/).

Acknowledgments
Support from the NSF Climate and Large-Scale Dynamics program (2039384 to LLH and 2039388 to TJG) and the NASA Living With a Star science program (80NSSC21K1309) is appreciated. The authors thank Zane Martin and C. Andrew Hoopes for assistance in implementing the method for calculating OMI MJO amplitudes from the MRI model data. Thanks to the anonymous reviewers for constructive criticisms of an earlier manuscript.

References

Abhik, S., & Hendon, H. H. (2019). Influence of the QBO on the MJO during coupled model multiweek forecasts. *Geophysical Research Letters*, *46*(15), 9213–9221. https://doi.org/10.1029/2019GL083152

Adames, A. F., & Kim, D. (2016). The MJO as a dispersive, convectively coupled moisture wave: Theory and observations. *Journal of the Atmospheric Sciences*, *73*(3), 913–941. https://doi.org/10.1175/JAS-D-15-0170.1

Andrews, D. G., Holton, J. R., & Leovy, C. B. (1987). *Middle atmosphere dynamics* (p. 489). Academic Press.

Baldwin, M. P., Gray, L. J., Dunkerton, T. J., Hamilton, K., Haynes, P. H., Randel, W. J., et al. (2001). The quasi-biennial oscillation. *Reviews of Geophysics*, *39*(2), 179–229. https://doi.org/10.1029/1999RG000073

Butler, A. H., Sjoberg, J. P., Seidel, D. J., & Rosenlof, K. H. (2017). A sudden stratospheric warming compendium. *Earth System Science Data*, *9*(1), 63–76. https://doi.org/10.5194/essd-9-63-2017

Chandra, S. (1986). The solar and dynamically induced oscillations in the stratosphere. *Journal of Geophysical Research*, *91*(D2), 2719–2734. https://doi.org/10.1029/JD091ID02P02719

Charlton, A. J., & Polvani, L. M. (2007). A new look at stratospheric sudden warmings. Part I: Climatology and modeling benchmarks. *Journal of Climate*, *20*(3), 449–469. https://doi.org/10.1175/JCLI3996.1

Charney, J. G., & Drazin, P. G. (1961). Propagation of planetary-scale disturbances from the lower into the upper atmosphere. *Journal of Geophysical Research*, *66*(1), 83–109. https://doi.org/10.1029/JZ066i001p00083

Chen, C. C., Richter, J. H., Liu, C., Moncrieff, M. W., Tang, Q., Lin, W., et al. (2021). Effects of organized convection parameterization on the MJO and precipitation in E3SMv1. Part I: Mesoscale heating. *Journal of Advances in Modeling Earth Systems*, *13*(6), e2020MS002401. https://doi.org/10.1029/2020MS002401

Elsbury, D., Peings, Y., & Magnusdottir, G. (2021). CMIP6 models underestimate the Holton-Tan effect. *Geophysical Research Letters*, *48*(24), e2021GL094083. https://doi.org/10.1029/2021GL094083

Eyring, V., Bony, S., Meehl, G. A., Senior, C. A., Stevens, B., Stouffer, R. J., & Taylor, K. E. (2016). Overview of the Coupled Model Intercomparison Project Phase 6 (CMIP6) experimental design and organization. *Geoscientific Model Development*, *9*(5), 1937–1958. https://doi.org/10.5194/gmd-9-1937-2016

Fritz, S., & Soules, S. D. (1970). Large-scale temperature changes in the stratosphere observed from Nimbus III. *Journal of the Atmospheric Sciences*, *27*(7), 1091–1097. https://doi.org/10.1175/1520-0469(1970)027<1091:LSTCIT>2.0.CO;2

Fueglistaler, S., Abalos, M., Flannaghan, T. J., Lin, P., & Randel, W. J. (2014). Variability and trends in dynamical forcing of tropical lower stratospheric temperatures. *Atmospheric Chemistry and Physics*, *14*(24), 13439–13453. https://doi.org/10.5194/acp-14-13439-2014

Garfinkel, C. I., Benedict, J. J., & Maloney, E. D. (2014). Impact of the MJO on the boreal winter extratropical circulation. *Geophysical Research Letters*, *41*(16), 6055–6062. https://doi.org/10.1002/2014GL061094

Garfinkel, C. I., Feldstein, S. B., Waugh, D. W., Yoo, C., & Lee, S. (2012). Observed connection between stratospheric sudden warmings and the Madden-Julian Oscillation. *Geophysical Research Letters*, *39*(18), L18807. https://doi.org/10.1029/2012GL053144

Giorgetta, M. A., Bengtsson, L., & Arpe, K. (1999). An investigation of QBO signals in the east Asian and Indian monsoon in GCM experiments. *Climate Dynamics*, *15*(6), 435–450. https://doi.org/10.1007/s003820050292

Gray, L. J., Brown, M. J., Knight, J., Andrews, M., Lu, H., O'Reilly, C., & Anstey, J. (2020). Forecasting extreme stratospheric polar vortex events. *Nature Communications*, *11*(1), 4630. https://doi.org/10.1038/s41467-020-18299-7

Gray, L. J., Crooks, S., Pascoe, C., Sparrow, S., & Palmer, M. (2004). Solar and QBO influences on the timing of stratospheric sudden warmings. *Journal of the Atmospheric Sciences*, *61*(23), 2777–2796. https://doi.org/10.1175/JAS-3297.1

Gray, L. J., Lu, H., Brown, M. J., Knight, J. R., & Andrews, M. B. (2022). Mechanisms of influence of the semi-annual oscillation on stratospheric sudden warmings. *Quarterly Journal of the Royal Meteorological Society*, *148*(744), 1223–1241. https://doi.org/10.1002/qj.4256

Haynes, P., Hitchcock, P., Hitchman, M., Yoden, S., Hendon, H., Kiladis, G., et al. (2021). The influence of the stratosphere on the tropical troposphere. *Journal of the Meteorological Society of Japan*, *99*(4), 803–845. https://doi.org/10.2151/jmsj.2021-040

Hendon, H. H., & Abhik, S. (2018). Differences in vertical structure of the Madden-Julian Oscillation associated with the quasi-biennial oscillation. *Geophysical Research Letters*, *45*(9), 4419–4428. https://doi.org/10.1029/2018GL077207

Hersbach, H., Bell, B., Berrisford, P., Hirahara, S., Horányi, A., Muñoz Sabater, J., et al. (2020). The era5 global reanalysis. *Quarterly Journal of the Royal Meteorological Society*, *146*(730), 1999–2049. https://doi.org/10.1002/qj.3803

Hoffmann, C. G., Kiladis, G. N., Gehne, M., & von Savigny, C. (2021). A Python package to calculate the OLR-based index of the Madden-Julian Oscillation (OMI) in climate science and weather forecasting. *Journal of Open Research Software*, *9*(1), 9. https://doi.org/10.5281/zenodo.3613752

Hoffmann, C. G., & von Savigny, C. (2019). Indications for a potential synchronization between the phase evolution of the Madden-Julian oscillation and the solar 27-day cycle. *Atmospheric Chemistry and Physics*, *19*(7), 4235–4256. https://doi.org/10.5194/acp-19-4235-2019

Holton, J. R., Haynes, P. H., McIntyre, M. E., Douglass, A., Rood, R., & Pfister, L. (1995). Stratosphere-troposphere exchange. *Reviews of Geophysics*, *33*(4), 403–439. https://doi.org/10.1029/95RG02097

Holton, J. R., & Tan, H.-C. (1980). The influence of the equatorial quasi-biennial oscillation on the global circulation at 50 mb. *Journal of the Atmospheric Sciences*, *37*(10), 2200–2208. https://doi.org/10.1175/1520-0469(1980)037<2200:TIOTEQ>2.0.CO;2

Holton, J. R., & Tan, H.-C. (1982). The quasi-biennial oscillation in the Northern Hemisphere lower stratosphere. *Journal of the Meteorological Society of Japan*, *60*(1), 140–148. https://doi.org/10.2151/jmsj1965.60.1_140

Hood, L. L. (2016). Lagged response of tropical tropospheric temperature to solar ultraviolet variations on intraseasonal time scales. *Geophysical Research Letters*, *43*(8), 4066–4075. https://doi.org/10.1002/2016GL068855

Hood, L. L. (2017). QBO/solar modulation of the boreal winter Madden-Julian oscillation: A prediction for the coming solar minimum. *Geophysical Research Letters*, *44*(8), 3849–3857. https://doi.org/10.1002/2017GL072832

Hood, L. L. (2018). Short-term solar modulation of the Madden-Julian climate oscillation. *Journal of the Atmospheric Sciences*, *75*(3), 857–873. https://doi.org/10.1175/JAS-D-17-0265.1

Hood, L. L., Redman, M., Johnson, W., & Galarneau, T. J., Jr. (2020). Stratospheric influences on the MJO-induced Rossby wave train: Effects on intraseasonal climate. *Journal of Climate*, *33*(1), 365–389. https://doi.org/10.1175/JCLI-D-18-0811.1

Hood, L. L., & Soukharev, B. (2003). Quasi-decadal variability of the tropical lower stratosphere: The role of extratropical wave forcing. *Journal of the Atmospheric Sciences*, *60*(19), 2389–2403. https://doi.org/10.1175/1520-0469(2003)060<2389;QVOTTL>2.0.CO;2

Karpechko, A. Y. (2018). Predictability of sudden stratospheric warmings in the ECMWF extended-range forecast system. *Monthly Weather Review*, *146*(4), 1063–1075. https://doi.org/10.1175/MWR-D-17-0317.1

Kiladis, G. N., Dias, J., Straub, K. H., Wheeler, M. C., Tulich, S. N., Kikuchi, K., et al. (2014). A comparison of OLR and circulation-based indices for tracking the MJO. *Monthly Weather Review*, *142*(5), 1697–1715. https://doi.org/10.1175/MWR-D-13-00301.1

Kim, H., Caron, J. M., Richter, J. H., & Simpson, I. R. (2020). The lack of QBO-MJO connection in CMIP6 models. *Geophysical Research Letters*, *47*(5), e2020GL087295. https://doi.org/10.1029/2020GL087295

Kodera, K. (2006). Influence of stratospheric sudden warming on the equatorial troposphere. *Geophysical Research Letters*, *33*(6), L06804. https://doi.org/10.1029/2005GL024510

Kodera, K., & Kuroda, Y. (2002). Dynamical response to the solar cycle. *Journal of Geophysical Research*, *107*(D24), 4749. https://doi.org/10.1029/2002JD002224

Labitzke, K. (1982). On the interannual variability of the middle stratosphere during the northern winters. *Journal of the Meteorological Society of Japan*, *60*(1), 124–138. https://doi.org/10.2151/JMSJ1965.60.1_124

Labitzke, K. (1987). Sunspots, the QBO, and the stratospheric temperature in the north polar region. *Geophysical Research Letters*, *14*(5), 535–537. https://doi.org/10.1029/1987GL7L6530

Labitzke, K., & van Loon, H. (1988). Associations between the 11-year solar cycle, the QBO and the atmosphere. Part I: The troposphere and stratosphere in the Northern Hemisphere in winter. *Journal of Atmospheric and Terrestrial Physics*, *50*(3), 197–206. https://doi.org/10.1016/0021-9169(88)90068-2

LaMorte, W. H. (2021). *Confidence intervals for sample size less than 30, PH717 Module 6 – Random error, probability, estimation, and confidence intervals*. Boston University School of Public Health. Retrieved from https://sphweb.bumc.bu.edu/otlt/MPH-Modules/PH717-Quant-Core/PH717-Module6-RandomError/PH717-Module6-RandomError11.html

Lee, J. C. K., & Klingaman, N. P. (2018). The effect of the quasi-biennial oscillation on the Madden-Julian oscillation in the Met Office Unified Model Global Ocean Mixed-Layer configuration. *Atmospheric Science Letters*, *19*(5), e816. https://doi.org/10.1002/asl.816

Lu, H., Hitchman, M. H., Gray, L. J., Anstey, J. A., & Osprey, S. M. (2020). On the role of Rossby wave breaking in the quasi-biennial modulation of the stratospheric polar vortex during boreal winter. *Quarterly Journal of the Royal Meteorological Society*, *146*(729), 1939–1959. https://doi.org/10.1002/qj.3775

Martin, Z., Orbe, C., Wang, S., & Sobel, A. H. (2021). The MJO-QBO relationship in a GCM with stratospheric nudging. *Journal of Climate*, *34*, 4603–4624. https://doi.org/10.1175/JCLI-D-20-0636.1

Martin, Z., Son, S.-W., Butler, A., Hendon, H., Kim, H., Sobel, A., et al. (2021). The influence of the quasi-biennial oscillation on the Madden-Julian oscillation. *Nature Reviews Earth & Environment*, *2*(7), 477–489. https://doi.org/10.1038/s43017-021-00173-9

Martin, Z., Vitart, F., Wang, S., & Sobel, A. (2020). The impact of the stratosphere on the MJO in a forecast model. *Journal of Geophysical Research: Atmospheres*, *125*(4), e2019JD032106. https://doi.org/10.1029/2019JD032106

Martin, Z., Wang, S., Nie, J., & Sobel, A. (2019). The influence of the quasi-biennial oscillation on the Madden-Julian oscillation in idealized cloud-resolving simulations. *Journal of the Atmospheric Sciences*, *76*(3), 669–688. https://doi.org/10.1175/JAS-D-18-0179.1

Matthews, A. J., Hoskins, B. J., & Masutani, M. (2004). The global response to tropical heating in the Madden-Julian oscillation during the northern winter. *Quarterly Journal of the Royal Meteorological Society*, *130*(7), 1991–2011. https://doi.org/10.1256/qj.02.123

Nishimoto, E., & Yoden, S. (2017). Influence of the stratospheric quasi-biennial oscillation on the Madden–Julian oscillation during austral summer. *Journal of the Atmospheric Sciences*, *74*(4), 1105–1125. https://doi.org/10.1175/JAS-D-16-0205.1

Randel, W. J. (1993). Global variations of zonal mean ozone during stratospheric warming events. *Journal of the Atmospheric Sciences*, *50*(19), 3308–3321. https://doi.org/10.1175/1520-0469(1993)050<3308.GVOZMO>2.0.CO;2

Randel, W. J., Garcia, R., & Wu, F. (2002). Time-dependent upwelling in the tropical lower stratosphere estimated from the zonal-mean momentum budget. *Journal of the Atmospheric Sciences*, *59*(13), 2141–2152. https://doi.org/10.1175/1520-0469(2002)059<2141:TDUITT>2.0.CO;2

Rao, J., Garfinkel, C. I., Chen, H., & White, I. P. (2019). The 2019 New Year stratospheric sudden warming and its real-time predictions in multiple S2S models. *Journal of Geophysical Research: Atmospheres*, *124*(21), 11155–11174. https://doi.org/10.1029/2019JD030826

Rao, J., Garfinkel, C. I., & White, I. P. (2020). Impact of the quasi-biennial oscillation on the northern winter stratospheric polar vortex in CMIP5/6 models. *Journal of Climate*, *33*(11), 4787–4813. https://doi.org/10.1175/JCLI-D-19-0663.s1

Sakaeda, N., Dias, J., & Kiladis, G. N. (2020). The unique characteristics and potential mechanisms of the MJO-QBO relationship. *Journal of Geophysical Research: Atmospheres*, *125*(17), e2020JD033196. https://doi.org/10.1029/2020JD033196

Silverman, V., Lubis, S. W., Harnik, N., & Matthes, K. (2021). A symoptic view of the onset of the midlatitude QBO signal. *Journal of the Atmospheric Sciences*, *78*, 3759–3780. https://doi.org/10.1175/JAS-D-20-0387.1

Sobel, A. H., & Maloney, E. (2012). An idealized semi-empirical framework for modeling the Madden-Julian oscillation. *Journal of the Atmospheric Sciences*, *69*(5), 1691–1705. https://doi.org/10.1175/JAS-D-11-0118.1

Toms, B. A., Barnes, E. A., Maloney, E. D., & van den Heever, S. C. (2020). The global teleconnection signature of the Madden-Julian oscillation and its modulation by the quasi-biennial oscillation. *Journal of Geophysical Research: Atmospheres*, *125*(7), e2020JD032653. https://doi.org/10.1029/2020JD032653

Wang, W., & Tziperman, E. (2018). The MJO-SSW teleconnection: Interaction between MJO-forced waves and the midlatitude jet. *Geophysical Research Letters*, *45*(9), 4400–4409. https://doi.org/10.1029/2018GL077937

Watson, P. A. G., & Gray, L. J. (2014). How does the quasi-biennial oscillation affect the stratospheric polar vortex? *Journal of the Atmospheric Sciences*, *71*(1), 391–409. https://doi.org/10.1175/JAS-D-13-096.1

White, I. P., Lu, H., & Mitchell, N. J. (2016). Seasonal evolution of the QBO-induced wave forcing and circulation anomalies in the northern winter stratosphere. *Journal of Geophysical Research: Atmospheres*, *121*(18), 10411–10431. https://doi.org/10.1002/2015JD024507

Yoo, D., & Son, S.-W. (2016). Modulation of the boreal wintertime Madden-Julian oscillation by the stratospheric quasi-biennial oscillation. *Geophysical Research Letters*, *43*(3), 1392–1398. https://doi.org/10.1002/2016GL067762

Yoshida, K., & Yamazaki, K. (2011). Tropical cooling in the case of stratospheric sudden warming in January 2009: Focus on the tropical tropopause layer. *Atmospheric Chemistry and Physics*, *11*(13), 6325–6336. https://doi.org/10.5194/acp-11-6325-2011

Yukimoto, S., Kawai, H., Koshiro, T., Oshima, N., Yoshida, K., Urakawa, S., et al. (2019). The Meteorological Research Institute Earth System Model version 2.0, MRI-ESM2.0: Description and basic evaluation of the physical component. *Journal of the Meteorological Society of Japan, Series II*, *97*(5), 931–965. https://doi.org/10.2151/jmsj.2019-051

Zhang, C. (2013). Madden-Julian Oscillation: Bridging weather and climate. *Bulletin of the American Meteorological Society*, *94*(12), 1849–1870. https://doi.org/10.1175/BAMS-D-12-00026.1

Zhang, C., & Zhang, B. (2018). QBO-MJO connection. *Journal of Geophysical Research: Atmospheres*, *123*(6), 2957–2967. https://doi.org/10.1002/2017JD028171